Int. J. Heat Mass Transfer. Vol. 22, pp. 1445–1454
Pergamon Press Ltd. 1979. Printed in Great Britain

INTERACTION BETWEEN SURFACE MASS TRANSFER AND TRANSVERSE CURVATURE IN NATURAL CONVECTION BOUNDARY LAYERS

W. J. MINKOWYCZ
Department of Energy Engineering, University of Illinois at Chicago Circle, Chicago, IL 60680, U.S.A.

and

E. M. SPARROW
Department of Mechanical Engineering, University of Minnesota, Minneapolis, MN 55455, U.S.A.

(*Received* 19 *December* 1978 *and in revised form* 16 *February* 1979)

Abstract—The heat transfer characteristics for natural convection about an isothermal vertical cylinder with surface mass transfer (blowing or suction) have been determined by analysis. The problem was formulated by applying the local nonsimilarity method, and solutions were obtained by a numerical scheme which employs integrated forms of the governing differential equations. Numerical solutions were carried out for a wide range of values of parameters which respectively characterize the transverse curvature of the cylinder and the magnitude and sign of the surface mass transfer. The Prandtl number was varied between 0.01 and 10. It was found that the local Nusselt numbers for a vertical cylinder are less sensitive to surface mass transfer than are those for a vertical plate. The sensitivity of both the cylinder and the plate Nusselt numbers to the mass transfer is diminished at low Prandtl numbers and increased at high Prandtl numbers.

NOMENCLATURE

F, reduced stream function, equation (6);
G, velocity function, $\partial F/\partial\xi$;
g, acceleration of gravity;
H, velocity function, $\partial G/\partial\xi$;
h, local heat transfer coefficient, $q/(T_w - T_\infty)$;
I_Ω, computational quantity, equation (32);
J_Ω, computational quantity, equation (33);
k, thermal conductivity;
M, surface mass transfer parameter, equation (13);
Nu, local Nusselt number, hx/k;
Nu_{fp}, flat plate Nusselt number;
Nu^*, Nusselt number for no surface mass transfer;
P, coefficients in governing equations;
Pr, Prandtl number;
Q, right-hand sides of governing equations;
q, local heat flux per unit time and area;
r, radial coordinate;
r_0, radius of cylinder;
T, temperature;
T_w, surface temperature;
T_∞, ambient temperature;
u, streamwise velocity;
v, transverse velocity;
v_w, transverse velocity at surface;
x, axial coordinate.

Greek symbols

α, thermal diffusivity;
β, thermal expansion coefficient;
η, pseudo-similarity variable, equation (4);
θ, dimensionless temperature, $(T - T_\infty)/(T_w - T_\infty)$;
Λ, prototype temperature function, equation (18);
ν, kinematic viscosity;
ξ, transformed streamwise coordinate, equation (5);
ϕ, temperature function, $\partial\theta/\partial\xi$;
χ, temperature function, $\partial\phi/\partial\xi$;
ψ, stream function;
Ω, prototype velocity function, equation (17).

INTRODUCTION

THE EFFECTS of surface mass transfer (blowing and suction) on natural convection adjacent to a vertical plate have been subjected to extensive study [1–9] and are now well understood. Basic to the results is the thickening (by blowing) or thinning (by suction) of the boundary layer that is caused by the surface mass transfer. The key role played by these changes in boundary layer thickness suggests that the flat plate results will not carry over to other cases where the layer thickness is either more or less responsive.

A case in point is the vertical cylinder, and the focus of the present paper is to study the effects of mass transfer on natural convection adjacent to such a geometry. Specific consideration is given to a cylinder whose surface is isothermal and to mass transfer that is uniformly distributed along the surface.

It is well established that in the absence of surface mass transfer, the natural convection boundary layer on a vertical cylinder is thinner than that on a vertical plate. This characteristic stems from the finite transverse curvature of the cylinder surface. It can be reasoned that the mechanisms which give rise to the thinner boundary layer on the cylinder will also alter the responsiveness of the boundary layer thickness to surface mass transfer. Consequently, it can be expected that the cylinder heat transfer results, when ratioed for the cases with and without surface mass transfer, will differ from the corresponding ratio for the flat plate.

Natural convection adjacent to an isothermal vertical cylinder does not admit a similarity-type boundary layer solution [10], and this state of affairs continues to prevail in the presence of surface mass transfer. To solve the latter problem, the local non-similarity solution method is used here. This method, first described in [11], has been employed to good effect for many non-similarity boundary layer problems, for example [12–14]. The main attributes of the method are that (a) solutions are obtainable at any given axial station without reference to other stations, (b) accuracy verifications can be made internal to the method, and (c) the equations that have to be solved are ordinary differential equations of the similarity type.

Numerical solutions of the governing differential equations generated by applying the local non-similarity method are obtained by employing a solution scheme described in [9]. That scheme is based on the use of integrated forms of the governing equations which incorporate the given boundary conditions. In order to make the solution scheme more effective in dealing with relatively thick boundary layers (e.g. low Prandtl number fluids), a modification of the scheme has been adopted here, as will be described later.

An examination of the governing equations and boundary conditions indicates the presence of three prescribable parameters: (a) the transverse curvature parameter ξ, (b) the surface mass transfer parameter M, and (c) the Prandtl number. Solutions were carried out for ξ values of 1, 2, and 5. All of these correspond to significant curvature effects as witnessed by the fact that for the no mass transfer case [10], the corresponding local heat transfer coefficients are 1.4, 1.75, and 2.65 times the flat plate value for $Pr \simeq 0.7$. For completeness, results for $\xi = 0$ (flat plate), including surface mass transfer, are also presented (these results are borrowed from [9]). For each ξ value, the surface mass transfer parameter M was assigned values to cover the range from -2.4 to 2.4, with positive M denoting blowing and negative M denoting suction. Finally, at each ξ and M, results were obtained for Prandtl numbers of 0.01, 0.72, 1, 2, 5, and 10.

It is relevant to note that the present results for $M = 0$ constitute an extension of the available information for natural convection on an isothermal vertical cylinder without mass transfer. Previously published solutions [10] for this case had been limited to $Pr \simeq 0.7$.

The results of the solutions are presented in both graphical and tabular form. The graphs, which correspond to representative Prandtl numbers, are plotted in terms of Nusselt number *ratios* to clearly portray mass transfer induced deviations from a reference state. In one set of graphs, the cylinder Nusselt numbers with and without mass transfer are ratioed at a fixed curvature and then plotted as a function of the mass transfer parameter. These graphs show the direct effect of the mass transfer on the Nusselt number for a given curvature. In a second set of graphs, the cylinder and flat plate Nusselt numbers are ratioed at a succession of fixed values of the mass transfer parameter. This comparison indicates the relative sensitivities of the cylinder and the flat plate to surface mass transfer.

The tables provide a listing of the dimensionless temperature and velocity derivatives at the cylinder surface for all of the cases that were investigated.

ANALYSIS

Problem formulation

The governing conservation equations for the velocity and temperature fields are expressed in cylindrical coordinates in which x, the axial coordinate, is vertically upward. The boundary layer form of these equations for a constant property fluid (with a linear density–temperature relationship for the buoyancy term) is

$$\frac{\partial}{\partial x}(ru) + \frac{\partial}{\partial r}(rv) = 0 \tag{1}$$

$$u\frac{\partial u}{\partial x} + v\frac{\partial u}{\partial r} = g\beta(T - T_\infty) + \frac{\nu}{r}\frac{\partial}{\partial r}\left(r\frac{\partial u}{\partial r}\right) \tag{2}$$

$$u\frac{\partial T}{\partial x} + v\frac{\partial T}{\partial r} = \frac{\alpha}{r}\frac{\partial}{\partial r}\left(r\frac{\partial T}{\partial r}\right). \tag{3}$$

Although these equations do not admit a similarity solution for the case of an isothermal vertical cylinder, it is advantageous to introduce a pseudo-similarity variable η along with a stretched axial coordinate ξ as follows

$$\eta = (g\beta(T_w - T_\infty)r_0^3/4\nu^2)^{1/4} \times (r^2/r_0^2 - 1)/2(x/r_0)^{1/4} \tag{4}$$

$$\xi = 2(x/r_0)^{1/4}/(g\beta(T_w - T_\infty)r_0^3/4\nu^2)^{1/4} \tag{5}$$

where T_w and T_∞ respectively denote the wall and ambient temperatures, and r_0 is the radius of the cylinder. The motivation for employing the trans-

formation (4), (5) is that the transformed conservation equations are much less dependent on the axial coordinate than are the original conservation equations.

To supplement the coordinate transformation given by equations (4) and (5), the dependent variables (velocities and temperature) are transformed by

$$\psi = 4\nu r_0 (x/r_0)^{3/4} \times (g\beta(T_w - T_\infty) r_0^3/4\nu^2)^{1/4} F(\xi, \eta) \quad (6)$$

$$(T - T_\infty)/(T_w - T_\infty) = \theta(\xi, \eta) \quad (7)$$

where $ru = \partial\psi/\partial r$, $rv = -\partial\psi/\partial x$.

When the transformation is applied to equations (2) and (3), there results

$$((1+\xi\eta)\mathrm{F}'')' + 3\mathrm{F}\mathrm{F}'' - 2(\mathrm{F}')^2 + \theta = \xi(\mathrm{F}'\partial\mathrm{F}'/\partial\xi - \mathrm{F}''\partial\mathrm{F}/\partial\xi) \quad (8)$$

$$(1/Pr)((1+\xi\eta)\theta')' + 3F\theta' = \xi(F'\partial\theta/\partial\xi - \theta'\partial F/\partial\xi) \quad (9)$$

in which $' = \partial/\partial\eta$. In equations (8) and (9), the presence of both ξ and η, as well as of derivatives in both these coordinates, confirms that similarity was not achieved by the transformation.

Attention will now be turned to the boundary conditions. The surface mass transfer will be expressed via the transverse velocity v_w at the surface of the cylinder, with blowing characterized by $v_w > 0$ and suction by $v_w < 0$. For uniform surface mass transfer, which is the case considered here, v_w is constant. The other boundary conditions are that $u = 0$ and $T = T_w$ at the cylinder surface and that $u = 0$ and $T = T_\infty$ in the ambient fluid. After transformation, the boundary conditions become

$$\text{at } \eta = 0\text{: } F = -(1/6)(\xi(v_w r_0/\nu) + 2\xi(\partial F/\partial\xi)) \quad (10)$$

$$F' = 0, \quad \theta = 1 \quad (11)$$

$$\text{at } \eta = \infty\text{: } F' = 0, \quad \theta = 0. \quad (12)$$

The quantity $(v_w r_0/\nu)$ is a dimensionless group which characterizes the magnitude and sign of the surface mass transfer. It may also be noted that the product $\xi(v_w r_0/\nu)$ is independent of r_0 and can, therefore, be employed as a surface mass transfer parameter for both the cylinder and the flat plate. Indeed, $\frac{1}{2}\xi(v_w r_0/\nu)$ was used in the flat plate studies reported in [7] and [9]. In view of the filial relationship between the flat plate and the cylinder and of the comparisons that will be made between the results of the two cases, $\frac{1}{2}\xi(v_w r_0/\nu)$ will be employed here to characterize the surface mass transfer. This group will be denoted by M, so that

$$M = \tfrac{1}{2}\xi(v_w r_0/\nu) = (v_w x/\nu)/(g\beta(T_w - T_\infty)x^3/4\nu^2)^{1/4}. \quad (13)$$

Solution

As noted earlier, the solution of equations (8) and (9) subject to the boundary conditions (10)–(12) will be obtained by applying the local nonsimilarity method. This method is well documented in the literature (see references cited in the Introduction) and need not be described here in detail. The basic aim of the method is to avoid having to solve the F, θ partial differential equations which govern the nonsimilarity problem by eliminating derivatives in ξ. When the elimination is performed in the F, θ equations themselves, then the method reduces to local similarity. However, the thrust of method is to delete ξ derivatives from equations that are subsidiary to the F, θ equations, thereby leaving the F, θ equations fully intact. The phrase *level of truncation* is used to describe where the ξ derivatives are eliminated.

With regard to the problem at hand, the first level of truncation (i.e. local similarity) corresponds to the deletion of the right-hand sides of equations (8) and (9) and of the term $\partial F/\partial\xi$ in equation (10). The resulting equations are free of ξ derivatives and may be treated as ordinary differential equations of the boundary layer type, with ξ and $\frac{1}{2}\xi(v_w r_0/\nu) = M$ regarded as parameters.

To prepare for the second level of truncation, new unknowns $G = \partial F/\partial\xi$ and $\phi = \partial\theta/\partial\xi$ are introduced, respectively in equations (8)–(10) and in equation (9). With these insertions, equations (8)–(12) are retained without approximation. Additional equations to cover the new unknowns G and ϕ are generated as follows: Firstly, equation (8) (with G included) is differentiated with respect to ξ, and the term $\partial/\partial\xi(F'G' - F''G)$ is deleted. Then, the ξ derivative of equation (9) (with ϕ included) is carried out, and $\partial/\partial\xi(F'\phi - \theta'G)$ is deleted. Next, the boundary condition (10) (with G included) is differentiated, and $\partial G/\partial\xi$ is deleted. Finally, the ξ derivatives of the other boundary conditions (11) and (12) are taken. These operations provide an additional set of equations for G and ϕ which have to be solved simultaneously with equations (8)–(12).

The equations corresponding to higher levels of truncation are generated by extending the procedure described in the foregoing. In the present study, solutions were obtained at the third level of truncation inasmuch as previous work on related problems has indicated high accuracy at that level. For the third level equations, additional functions $H = \partial G/\partial\xi = \partial^2 F/\partial\xi^2$ and $\chi = \partial\phi/\partial\xi = \partial^2\theta/\partial\xi^2$ are introduced to supplement F, G, θ, *and* ϕ.

The surface mass transfer boundary condition (10) represents a special feature of the present study and, therefore, it is appropriate to show the forms which it takes at the various levels of truncation. At the first, second, and third levels, respectively

$$F = -M/3 \quad (14)$$

$$F = -M/4, \quad G = -M/4\xi \quad (15)$$

$$F = -M/4, \quad G = -M/4\xi, \quad H = 0 \quad (16)$$

where M is given by equation (13).

The numerical scheme described in [9] was employed here to solve the sets of differential equations that were generated by the local nonsimilarity method. The scheme is based on restating the differential equations in integrated form in such a way that the boundary conditions are already satisfied. To accomplish the restatement, the differential equations for the velocity functions (i.e. F, G, H, ...) are expressed in the form

$$\Omega''' + P_\Omega \Omega'' = Q_\Omega \tag{17}$$

while those for the temperature functions (θ, ϕ, χ, ...) are written as

$$\Lambda'' + P_\Lambda \Lambda' = Q_\Lambda. \tag{18}$$

Thus, for example, at the third level of truncation

$$F''' + P_F F'' = Q_F,\ \theta'' + P_\theta \theta' = Q_\theta \tag{19}$$

$$G''' + P_G G'' = Q_G,\ \phi'' + P_\phi \phi' = Q_\phi \tag{20}$$

$$H''' + P_H H'' = Q_H,\ \chi'' + P_\chi \chi' = Q_\chi \tag{21}$$

where

$$P_F = P_G = (3F + \xi + \xi G)/(1 + \xi\eta) \tag{22}$$

$$P_H = (3F + \xi)/(1 + \xi\eta) \tag{23}$$

$$P_\theta = P_\phi = (3PrF + \xi + Pr\xi G)/(1 + \xi\eta) \tag{24}$$

$$P_\chi = (3PrF + \xi)/(1 + \xi\eta) \tag{25}$$

$$Q_F = (2(F')^2 - \theta + \xi F'G')/(1 + \xi\eta) \tag{26}$$

$$Q_G = (5F'G' - 4F''G - \eta F''' - F'' - \phi + \xi(F'H' + (G')^2 - F''H))/(1 + \xi\eta) \tag{27}$$

$$Q_H = (6F'H' - 5F''H + 6(G')^2 - (8G + 2)G'' - 2\eta G''' - \chi)/(1 + \xi\eta) \tag{28}$$

$$Q_\theta = Pr\xi F'\phi/(1 + \xi\eta) \tag{29}$$

$$Q_\phi = (PrF'\phi - 4PrG\theta' - \eta\theta'' - \theta' + Pr\xi(F'\chi + G'\phi - \theta'H))/(1 + \xi\eta) \tag{30}$$

$$Q_\chi = (2PrF'\chi + 2Pr\phi G' - (8PrG + 2)\phi' - 2\eta\phi'' - 5Pr\theta'H))(1 + \xi\eta). \tag{31}$$

Once the P and Q functions and the boundary conditions have been identified, all of the necessary inputs are available to employ the numerical scheme of [9]. The description of the scheme given in [9] is sufficiently complete so that there is no need for reiteration here. It is, however, appropriate to describe a modification that was introduced here in order to circumvent difficulties which arise at large ξ values such as those that are encountered in the low Prandtl number flows and/or at large ξ.

In the numerical scheme, the following integrals have to be evaluated

$$I_\Omega(z) = \exp\left[-\int_0^z P_\Omega(\hat{z})\,\mathrm{d}\hat{z} \right] \tag{32}$$

$$J_\Omega(z) = \exp\left[\int_0^z P_\Omega(\hat{z})\,\mathrm{d}\hat{z} \right] \tag{33}$$

and similarly for I_Λ and J_Λ. If P is positive and z is large, it is seen from equation (33) that exp will take on tremendous values—values that are well beyond the capacity of a computer.

To avoid this difficulty, a term whose original form was

$$I_\Omega(\eta)\left[\int_0^\eta Q_\Omega(\hat{\eta}) J_\Omega(\hat{\eta})\,\mathrm{d}\hat{\eta} \right] \tag{34}$$

is rewritten as

$$\int_0^\eta Q_\Omega(\hat{\eta}) I_\Omega(\eta) J_\Omega(\hat{\eta})\,\mathrm{d}\hat{\eta} \tag{35}$$

and the IJ product evaluated as

$$I_\Omega(\eta)J_\Omega(\hat{\eta}) = \exp\left[-\int_0^\eta P_\Omega(\hat{\eta})\,\mathrm{d}\hat{\eta} + \int_0^{\hat{\eta}} P_\Omega(\hat{\eta})\,\mathrm{d}\hat{\eta} \right]. \tag{36}$$

Because of the competition between the two contributing terms, the argument of exp in equation (36) is always sufficiently small so that exp never overflows.

For η values where overflow is not an issue, much less computational time is required to evaluate equation (34) than to evaluate equation (35). Therefore, to minimize the overall expenditure of computer time, equation (34) was employed for all η values except for those where overflow would have occurred, and for those η values (35) was employed. The break point between the use of equations (34) and (35) was identified from auxiliary evaluations of equation (33), which established whether or not overflow occurred and, if overflow did occur, the corresponding η value was determined. For the majority of the cases treated here, it was possible to employ equation (34) in the calculations.

RESULTS AND DISCUSSION

The numerical solutions were carried out for wide ranges of the three prescribable parameters ξ, Pr, and M. For ξ, solutions were obtained for values of 1, 2, and 5. The results from these solutions will be supplemented by those for $\xi = 0$ from [9] in order to span the entire range from no transverse curvature ($\xi = 0$) to appreciable transverse curvature ($\xi = 5$). For the Prandtl number Pr, values of 0.01, 0.72, 1, 2, 5, and 10 were employed. Except for $Pr = 10$, values of the mass transfer parameter M equal to -2.4, -1.6, -0.8, 0, 0.8, 1.6, and 2.4 were assigned. Owing to the rapid drop off of the heat transfer with increasing positive M at $Pr = 10$, solutions were obtained for a somewhat finer subdivision of M between 0 and 1.2, and the $M = 1.6$ and 2.4 cases were not run.

The main focus of the presentation of results will be the local heat transfer coefficient h and its dimensionless counterpart, the local Nusselt number, respectively defined as

$$h = \frac{q}{T_w - T_\infty}, \quad Nu = \frac{hx}{k} \tag{37}$$

Table 1. Values of $-\theta'(\xi,0)$ for the third level of truncation

		Pr					
ξ	M	0.01	0.72	1.0	2.0	5.0	10.0
0.0	−2.4	0.9230(−1)*	1.746	2.404	4.800	12.00	24.00
	−1.6	0.8849(−1)	1.247	1.657	3.204	8.000	16.00
	−0.8	0.8460(−1)	0.8311	1.035	1.744	4.012	8.000
	0.0	0.8056(−1)	0.5046	0.5671	0.7165	0.9540	1.169
	0.8	0.7631(−1)	0.2701	0.2604	0.2011	0.7126(−1)	0.1046(−1)
	1.6	0.7182(−1)	0.1221	0.09400	0.03323	0.1067(−2)	0.1670†
	2.4	0.6713(−1)	0.04421	0.02461	0.2648(−2)	0.2058(−5)	0.2604(−3)‡
1.0	−2.4	0.2563	1.845	2.457	4.801	12.00	24.00
	−1.6	0.2523	1.401	1.786	3.244	8.000	16.00
	−0.8	0.2483	1.020	1.218	1.896	4.056	8.001
	0.0	0.2441	0.7067	0.7716	0.9257	1.169	1.388
	0.8	0.2398	0.4616	0.4472	0.3634	0.1584	0.3363(−1)
	1.6	0.2354	0.2814	0.2334	0.1099	0.8770(−2)	0.2832†
	2.4	0.2309	0.1585	0.1078	0.02446	0.1880(−3)	0.2301(−2)‡
2.0	−2.4	0.3987	1.966	2.550	4.813	12.00	24.00
	−1.6	0.3947	1.551	1.923	3.319	8.000	16.00
	−0.8	0.3906	1.189	1.387	2.050	4.128	8.004
	0.0	0.3864	0.8829	0.9516	1.113	1.365	1.590
	0.8	0.3822	0.6321	0.6171	0.5213	0.2604	0.7033(−1)
	1.6	0.3779	0.4347	0.3758	0.2068	0.2713(−1)	0.4079†
	2.4	0.3734	0.2861	0.2134	0.06833	0.1550(−2)	0.8230(−2)‡
5.0	−2.4	0.7932	2.344	2.884	4.960	12.00	24.00
	−1.6	0.7892	1.973	2.329	3.622	8.031	16.00
	−0.8	0.7851	1.638	1.841	2.493	4.431	8.067
	0.0	0.7810	1.342	1.422	1.607	1.889	2.134
	0.8	0.7768	1.083	1.072	0.9666	0.6035	0.2422
	1.6	0.7726	0.8599	0.7881	0.5405	0.1441	0.7998†
	2.4	0.7684	0.6719	0.5640	0.2804	0.2617(−1)	0.6008(−1)‡

*$0.9230(-1) = 0.9230 \times 10^{-1}$.
†$M = 0.4$.
‡$M = 1.2$.

where q, the local heat flux, is given by

$$q = k(T_w - T_\infty) \times (g\beta(T_w - T_\infty)/4xv^2)^{1/4}(-\theta'(\xi,0)). \quad (38)$$

By combining equations (37) and (38), there follows

$$Nu = (-\theta'(\xi,0))(Gr/4)^{1/4} \quad (39)$$

where Gr is the local Grashof number $g\beta(T_w - T_\infty)x^3/v^2$.

The dimensionless temperature derivative at the cylinder surface, $\theta'(\xi,0)$, which is the key quantity in the heat transfer results, depends on all three of the prescribable parameters, ξ, M, and Pr. A listing of the $\theta'(\xi,0)$ values obtained from the solutions at the third level of truncation is presented in Table 1. In the table, the ξ and M parameters are respectively indicated in the first and second columns of the table while the parametric values of the Prandtl number are deployed across the top of the table.

To clearly portray the effects of surface mass transfer, the Nusselt number results will be presented graphically in ratio form with respect to certain reference quantities. One of the reference quantities is the Nusselt number Nu^* for the case of no surface mass transfer, that is

$$Nu \equiv Nu^* \text{ for } M = 0. \quad (40)$$

The other reference quantity is the flat plate Nusselt number,

$$Nu \equiv Nu_{fp} \text{ for } \xi = 0. \quad (41)$$

With these reference quantities, two ratios will be formed. The first, Nu/Nu^*, compares the Nusselt numbers with and without surface mass transfer for a fixed value of the curvature parameter ξ and at a given Prandtl number. The second ratio is Nu/Nu_{fp}. It compares the cylinder and flat plate Nusselt numbers at the same value of the surface mass transfer parameter and at the same Prandtl number.

The Nu/Nu^* results are presented in Figs. 1 and 2. The first of these figures conveys results for $Pr = 0.01$ (upper graph) and for $Pr = 0.72$ (lower graph), while the second figure is for $Pr = 10$. These Prandtl numbers span the full range that was investigated here. In each figure, Nu/Nu^* is plotted as a function of the mass transfer parameter M. The range of M in Fig. 1 extends from -2.4 (strong suction) through zero (no surface mass transfer) to 2.4 (strong blowing). In Fig. 2, the abscissa range was truncated at $M = 0.8$ because of the rapid drop-off of Nu/Nu^* for positive M at $Pr = 10$. The curves are parameterized by the transverse curvature ξ.

Since $Nu/Nu^* = 1$ when $M = 0$, the departure of the curves from unity is a direct measure of the effect

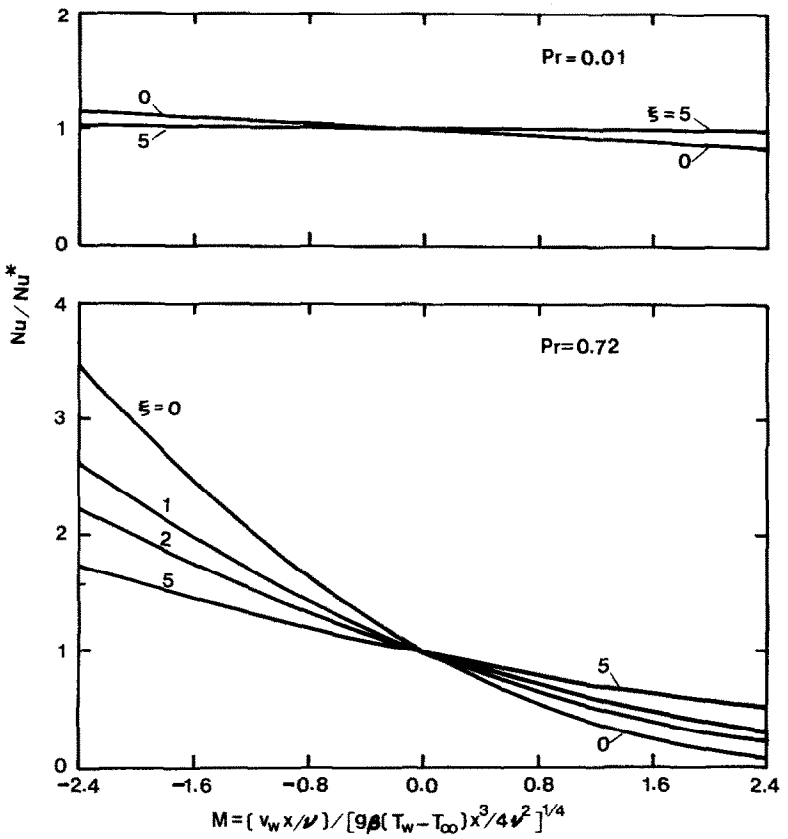

FIG. 1. Comparison of Nusselt numbers with and without surface mass transfer for fixed values of the curvature parameter, $Pr = 0.01$ and 0.72.

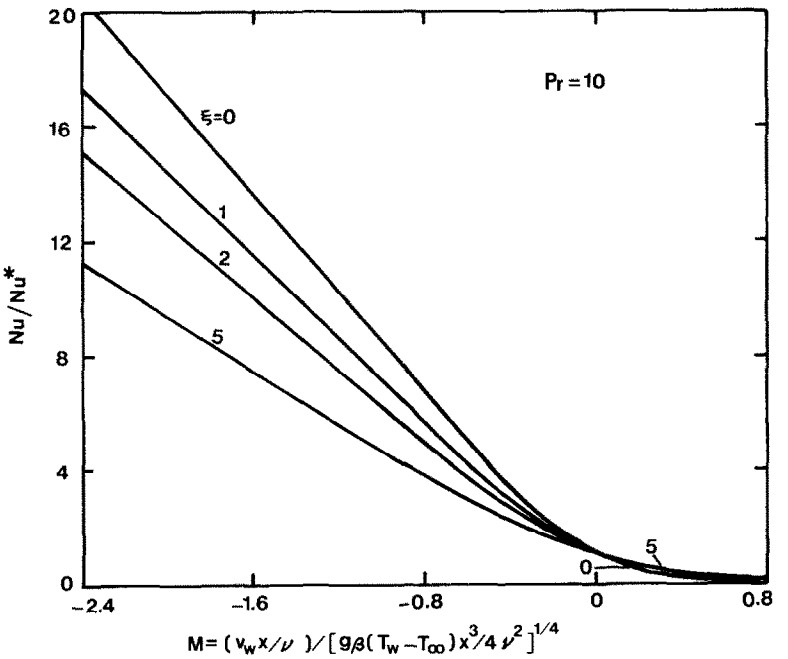

FIG. 2. Comparison of Nusselt numbers with and without surface mass transfer for fixed values of the curvature parameter, $Pr = 10$.

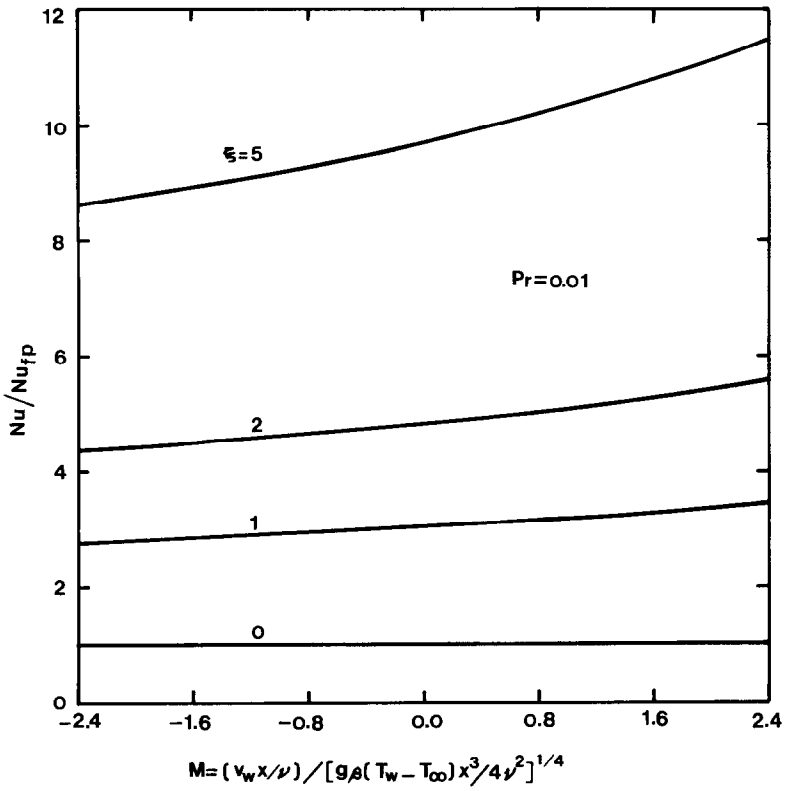

FIG. 3. Comparison of cylinder and flat plate Nusselt numbers, $Pr = 0.01$.

of surface mass transfer on the local heat transfer coefficient. As expected, suction ($M < 0$) increases the transfer coefficient and blowing ($M > 0$) decreases the transfer coefficient. Apart from this qualitative characteristic which is common to all cases, the extent of the mass transfer influence is markedly different depending on the Prandtl number and on the curvature parameter. At $Pr = 0.01$, Fig. 1 shows that at any fixed curvature ξ, the Nusselt number is only slightly affected by surface mass transfer. With increasing Prandtl number, the influence of surface mass transfer becomes more marked so that at $Pr = 0.72$ and, even to a greater extent at $Pr = 10$, there are major variations of Nu/Nu^* with M.

It is also seen from Figs. 1 and 2 that the role of transverse curvature is amplified with increasing Prandtl number. Whereas at $Pr = 0.01$ the curves for the various ξ values fall so close together that some had to be omitted to preserve clarity, there is a notable spread among the curves at higher Prandtl numbers. In general, the smaller the ξ value, the greater is the effect of surface mass transfer. Thus, the flat plate Nusselt numbers are most sensitive to surface mass transfer and those for small diameter cylinders are least sensitive.

The important role of the Prandtl number that was identified in the foregoing appears plausible when note is taken of the large variations of the boundary layer thickness with Prandtl number. In low Prandtl number fluids, the boundary layer is very thick and, as a consequence, the surface mass transfer only affects the inner part of the boundary layer. On the other hand, the thermal boundary layer for natural convection in high Prandtl number fluids is very thin, and the entire boundary layer is strongly affected by the surface mass transfer.

The lesser sensitivity of the cylinder to surface mass transfer (compared with the flat plate) is also physically plausible. To provide further perspectives about the relationship between the cylinder and the flat plate, Figs. 3, 4, and 5 have been prepared, respectively, for $Pr = 0.01$, 0.72, and 10. In each figure, the Nu/Nu_{fp} ratio is plotted as a function of the mass transfer parameter M, and the curves are labeled according to the curvature parameter ξ. In the ratio, both Nu and Nu_{fp} correspond to the same value of M.

From an overview of these figures, it is seen that for all cases, the ratio of the cylinder Nusselt number to that for the flat plate is larger in the presence of blowing than in the presence of suction. The differences between the Nu/Nu_{fp} ratios for blowing and suction become more marked as the Prandtl number increases. For $Pr = 0.01$, Nu/Nu_{fp} is generally large (i.e. well in excess of unity) for both suction and blowing, and there is only a modest increase as M increases. On the other hand, for higher Prandtl numbers, the cylinder and flat plate Nusselt numbers are very nearly the same for a range of suction values. This range grows wider with increasing Prandtl number, as witnessed by the line

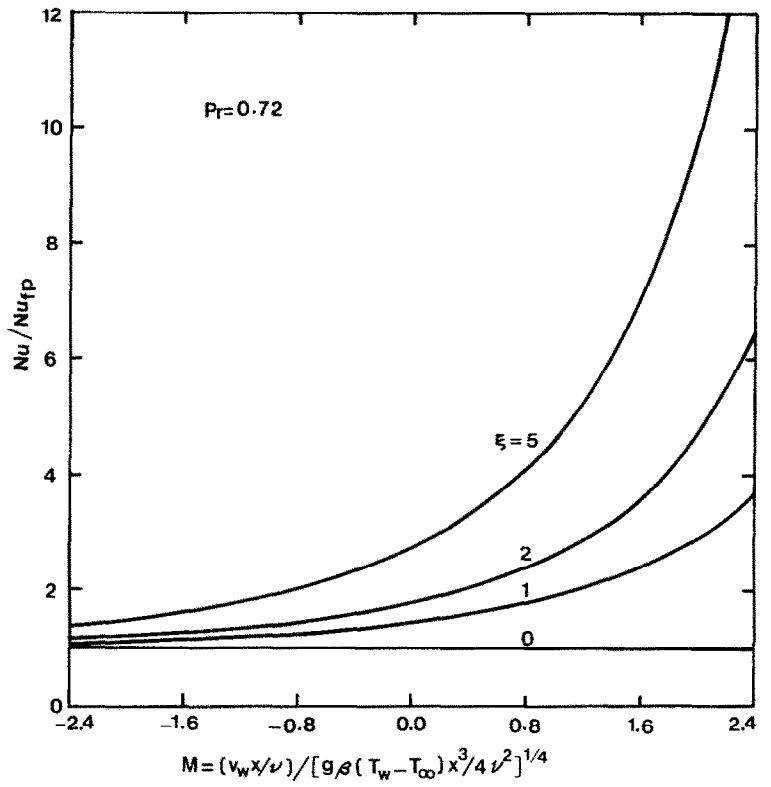

FIG. 4. Comparison of cylinder and flat plate Nusselt numbers, $Pr = 0.72$.

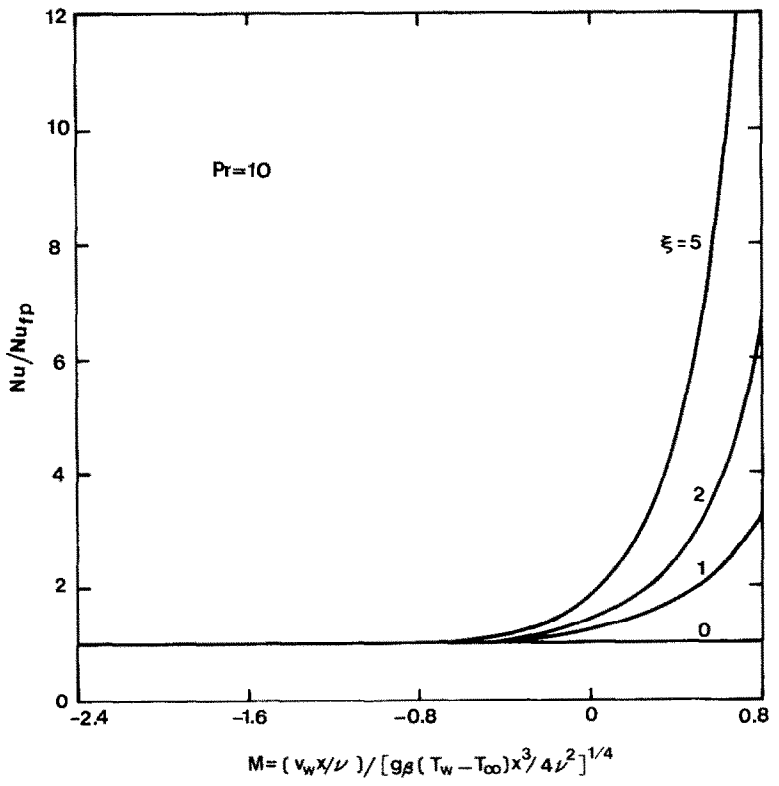

FIG. 5. Comparison of cylinder and flat plate Nusselt numbers, $Pr = 10$.

Table 2. Values of $f''(\xi, 0)$ for the third level of truncation

		Pr					
ξ	M	0.01	0.72	1.0	2.0	5.0	10.0
0.0	−2.4	1.953	0.5568	0.4139	0.2083	0.8322(−1)*	0.4166(−1)
	−1.6	1.613	0.6689	0.5497	0.3106	0.1250	0.6249(−1)
	−0.8	1.286	0.7095	0.6368	0.4722	0.2461	0.1250
	0.0	0.9872	0.6760	0.6422	0.5712	0.4818	0.4192
	0.8	0.7328	0.5920	0.5824	0.5689	0.5668	0.5725
	1.6	0.5351	0.4873	0.4881	0.4934	0.5015	0.1670†
	2.4	0.3962	0.3875	0.3899	0.3944	0.3971	0.2604(−3)‡
1.0	−2.4	1.975	0.7396	0.5722	0.2627	0.9089(−1)	0.4348(−1)
	−1.6	1.654	0.7844	0.6649	0.4004	0.1427	0.6665(−1)
	−0.8	1.352	0.7771	0.7030	0.5343	0.2930	0.1416
	0.0	1.078	0.7271	0.6886	0.6083	0.5084	0.4395
	0.8	0.8412	0.6482	0.6338	0.6118	0.6042	0.6111
	1.6	0.6459	0.5556	0.5544	0.5593	0.5736	0.2832†
	2.4	0.4940	0.4627	0.4666	0.4773	0.4873	0.2301(−2)‡
2.0	−2.4	1.993	0.8450	0.6809	0.3363	0.9986(−1)	0.4544(−1)
	−1.6	1.694	0.8559	0.7389	0.4718	0.1650	0.7123(−1)
	−0.8	1.414	0.8307	0.7549	0.5828	0.3338	0.1608
	0.0	1.159	0.7755	0.7328	0.6441	0.5343	0.4594
	0.8	0.9342	0.7001	0.6810	0.6504	0.6357	0.6419
	1.6	0.7425	0.6140	0.6098	0.6110	0.6279	0.4079†
	2.4	0.5854	0.5262	0.5295	0.5425	0.5596	0.8230(−2)‡
5.0	−2.4	2.070	1.038	0.8803	0.5217	0.1379	0.5220(−1)
	−1.6	1.816	1.012	0.8944	0.6235	0.2525	0.8831(−1)
	−0.8	1.577	0.9677	0.8849	0.6996	0.4337	0.2277
	0.0	1.356	0.9087	0.8548	0.7432	0.6073	0.5161
	0.8	1.155	0.8390	0.8079	0.7529	0.7149	0.7142
	1.6	0.9746	0.7627	0.7483	0.7328	0.7454	0.7998†
	2.4	0.8163	0.6839	0.6810	0.6888	0.7177	0.6008(−1)‡

*$0.8322(-1) = 0.8322 \times 10^{-1}$.
†$M = 0.4$.
‡$M = 1.2$.

$Nu/Nu_{fp} = 1$ which represents the results for most of the negative M values in Fig. 5. Furthermore, for these higher Prandtl numbers, the curves rise sharply in the presence of blowing and attain high values of Nu/Nu_{fp}. The sharpness of the rise is accentuated when the curvature of the cylinder is greater (i.e. higher ξ).

In interpreting the results of Figs. 3–5, it should be noted that both Nu and Nu_{fp} decrease with increasing M. Since Nu/Nu_{fp} increases with M, it follows that Nu_{fp} decreases more rapidly than does Nu. This confirms the conclusion already drawn from Figs. 1 and 2 that the flat plate is more sensitive to surface mass transfer than is the cylinder. This difference in sensitivity occurs because the annular boundary layer surrounding a cylinder can disperse and diffuse injected fluid more readily than can a plane boundary layer and, similarly, it can give up withdrawn fluid with lesser disruption. The ability to accommodate injected fluid is especially important at higher Prandtl numbers, where it serves to stave off the catastrophic decrease in Nusselt number with increased blowing that occurs for the flat plate.

To close the presentation of results, special attention may be called to the tabulated values of $\theta'(\xi, 0)$ for $M = 0$ and $\xi > 0$. These results correspond to cylinders without surface mass transfer. In view of the fact that the only previously published results for the isothermal cylinder were limited to $Pr \simeq 0.7$ [10], the $\theta'(\xi, 0)$ values given in Table 1 for other Prandtl numbers constitute new information. For completeness, the numerical values of $F''(\xi, 0)$ are listed in Table 2. In certain methods of solution, $F''(\xi, 0)$ and $\theta'(\xi, 0)$ are key quantities because they are starting values in a forward numerical integration.

CONCLUDING REMARKS

The solutions obtained here provide further confirmation of the effectiveness of the local nonsimilarity method for solving boundary layer problems. Special note should be taken, however, of the important role played by the adopted numerical scheme in the actual attainment of the solutions. This scheme, which is based on the use of integrated forms of the governing differential equations, yielded solutions for all of the selected parameter values, without undue difficulties being encountered. To cope with computer overflow which would have occurred in the solutions for thick boundary layers, a modification of the numerical scheme was devised and described in the paper.

The results of the analysis demonstrated that the local Nusselt numbers for a vertical cylinder are less

sensitive to surface mass transfer than are those for a vertical plate. The sensitivity of both the cylinder and the plate to the mass transfer is lessened at low Prandtl numbers and heightened at high Prandtl numbers.

REFERENCES

1. R. Eichhorn, The effect of mass transfer on free convection, *ASME J. Heat Transfer* **82**, 260–263 (1960).
2. E. M. Sparrow and R. D. Cess, Free convection with blowing or suction, *ASME J. Heat Transfer* **83**, 387–389 (1961).
3. I. Mabuchi, The effect of blowing or suction on heat transfer by free convection from a vertical plate, *Bull. JSME* **6**, 223–230 (1963).
4. P. M. Brdlik and V. A. Mochalov, Porous blowing and suction during free convection at a vertical surface, *Int. Chem. Engng* **5**, 603–607 (1965).
5. P. M. Brdlik and V. A. Mochalov, Experimental study of free convection with porous blowing and suction on a vertical surface, *J. Engng Phys.* **10**, 3–10 (1966).
6. J. F. Clarke, Transpiration and natural convection: the vertical flat plate problem, *J. Fluid Mech.* **57**, 45–61 (1973).
7. P. G. Parikh, R. J. Moffat, W. M. Kays and D. Bershader, Free convection over a vertical porous plate with transpiration, *Int. J. Heat Mass Transfer*, **17**, 1465–1474 (1974).
8. J. H. Merkin, The effects of blowing and suction on free convection boundary layers, *Int. J. Heat Mass Transfer* **18**, 237–244 (1975).
9. W. J. Minkowycz and E. M. Sparrow, Numerical solution scheme for local nonsimilarity boundary layer analysis, *Num. Heat Transfer* **1**, 69–85 (1978).
10. W. J. Minkowycz and E. M. Sparrow, Local nonsimilar solutions for natural convection on a vertical cylinder, *ASME J. Heat Transfer* **96**, 178–183 (1974).
11. E. M. Sparrow, H. Quack and C. J. Boerner, Local nonsimilarity boundary layer solutions, *AIAA J.* **8**, 1936–1942 (1970).
12. T. S. Chen and A. Mucoglu, Buoyancy effects on forced convection along a vertical cylinder, *ASME J. Heat Transfer* **97**, 198–203 (1975).
13. J. L. Novotny, J. D. Bankston and J. R. Lloyd, Local nonsimilarity applied to free convection boundary layers with radiation interaction, *Prog. Astronautics Aeronautics* **39**, 309–330 (1975).
14. C. C. Chen and R. Eichhorn, Natural convection from a vertical surface to a thermally stratified fluid, *ASME J. Heat Transfer* **98**, 446–451 (1976).

INTERACTION ENTRE LE TRANSFERT MASSIQUE A LA SURFACE ET LA COURBURE TRANSVERSALE DANS LES COUCHES LIMITES DE CONVECTION NATURELLE

Résumé—On détermine analytiquement les caractéristiques du transfert thermique par convection naturelle autour d'un cylindre vertical isotherme avec transfert massique (soufflage ou aspiration). Le problème est formulé en appliquant la méthode de non-similitude locale et les solutions sont obtenues par une méthode numérique qui emploie des formes intégrées des équations aux dérivées partielles. Des solutions numériques sont obtenues pour un large domaine de variation des paramètres qui caractérisent la courbure transversale du cylindre, et la grandeur et le signe du transfert massique à la surface. Le nombre de Prandtl varie entre 0,01 et 10. On trouve que le nombre de Nusselt local pour un cylindre vertical est moins sensible au transfert massique que pour une plaque verticale. La sensibilité, au transfert massique, des nombres de Nusselt pour le cylindre et pour la plaque est diminuée aux faibles nombres de Prandtl et augmentée pour les forts nombres de Prandtl.

WECHSELWIRKUNG ZWISCHEN STOFFÜBERGANG AN DER OBERFLÄCHE UND DEREN KRÜMMUNG IN QUERRICHTUNG IN GRENZSCHICHTEN BEI FREIER KONVEKTION

Zusammenfassung—Das Wärmeübergangsverhalten an einem isothermen vertikalen Zylinder mit Stoffübergang an der Oberfläche (Ausblasen oder Absaugen) ist rechnerisch bestimmt worden. Das Problem wurde mit Hilfe der Methode örtlicher Nichtähnlichkeit formuliert. Man erhielt Lösungen mittels eines numerischen Verfahrens, bei welchem die integrierte Form der beschreibenden Differentialgleichungen verwendet wurde. Numerische Lösungen wurden für einen weiten Bereich von Parametern ermittelt, welche die Querkrümmung des Zylinders sowie Größe und Vorzeichen des Stoffübergangs an der Oberfläche charakterisieren. Die Prandtl-Zahl wurde zwischen 0,01 und 10 variiert. Es zeigte sich, daß die örtlichen Nußelt-Zahlen für einen vertikalen Zylinder weniger stark vom Stoffübergang abhängen, als das bei einer ebenen Platte der Fall ist. Die Abhängigkeit der Nußelt-Zahlen vom Stoffübergang nimmt sowohl beim Zylinder als auch bei der ebenen Platte mit niedrigen Prandtl-Zahlen ab und steigt mit hohen.

ВЗАИМОДЕЙСТВИЕ МЕЖДУ ПЕРЕНОСОМ МАССЫ НА ПОВЕРХНОСТИ И ПОПЕРЕЧНОЙ КРИВИЗНОЙ В ЕСТЕСТВЕННОКОНВЕКТИВНЫХ ПОГРАНИЧНЫХ СЛОЯХ

Аннотация — Аналитическим путём определены характеристики переноса тепла естественной конвекцией у изотермического вертикального цилиндра при наличии переноса массы на его поверхности (вдув или отсос). Задача сформулирована с помощью метода локальной неавтомодельности. Её решения получены с использованием численной схемы и интегральных форм исходных дифференциальных уравнений. Численный расчёт проведен для широкого диапазона значений параметров, характеризующих соответственно поперечную кривизну цилиндра, а также величину и направление массопереноса на поверхности. Числа Прандтля изменялись от 0,01 до 10. Найдено, что локальные значения числа Нуссельта для вертикального цилиндра, по сравнению с вертикальной пластиной, меньше зависят от переноса массы на поверхности. Эта зависимость (для цилиндра и для пластины) ослабляется с уменьшением значения числа Прандтля и усиливается с его ростом.